ACCSCIENCE PUBLISHING

International Journal of Bioprinting

RESEARCH ARTICLE

Increased stiffness of extracellular matrix enhanced chemoresistance in 3D-bioprinted ovarian cancer model

Ying Shan[1†], Mingchang Pang[2†], Liqian Wang[3†], Yixin Mao[4†], Ruiyi Yan[2], Chang Zhou[5], Jingyuan Ji[5], Yilei Mao[2], Ying Jin[1*], and Huayu Yang[2*]

[1] Department of Obstetrics and Gynecology, National Clinical Research Center for Obstetric & Gynecologic Diseases, Peking Union Medical College Hospital, Chinese Academy of Medical Sciences & Peking Union Medical College, Beijing, China

[2] Department of Liver Surgery, Peking Union Medical College Hospital, Chinese Academy of Medical Sciences & Peking Union Medical College, Beijing, China

[3] Department of Gynecology, The Affiliated Yantai Yuhuangding Hospital of Qingdao University, Yantai, China

[4] Department of Geriatrics, Shanghai Eighth Peoples Hospital, Shanghai, China

[5] Biomanufacturing Center, Department of Mechanical Engineering, Tsinghua University, Beijing, China

(This article belongs to the *Special Issue: Bioprinting process for tumor model development*)

Abstract

Ovarian cancer is a gynecological malignancy with a high mortality rate. The ovarian cancer microenvironment is a crucial factor affecting the overall and progression-free survival rates of patients with ovarian cancer. The biophysical factors of the tumor microenvironment, such as stiffness, can affect the gene expression and behavior of tumor cells. In this study, we utilized 3D bioprinting technology to construct ovarian cancer tumor models with varying levels of stiffness *in vitro* to investigate the effect of extracellular matrix stiffness on drug resistance of tumor cells. Our findings indicate that increasing the stiffness of extracellular matrix can attenuate the sensitivity of tumor cells to chemotherapeutic agents. Additionally, the increased stiffness of 3D tumor model may promote malignant phenotypes, such as tumor stemness and tumor progression.

Keywords: 3D bioprinting technology; Ovarian cancer; Tumor microenvironment; Stiffness; Drug resistance

†These authors contributed equally to this work.

***Corresponding authors:**
Huayu Yang (dolphinyahy@hotmail.com)

Ying Jin (jinying@pumch.cn)

Citation: Shan Y, Pang M, Wang L, et al. Increased stiffness of extracellular matrix enhanced chemoresistance in 3D-bioprinted ovarian cancer model. *Int J Bioprint*. 2024;10(3):1673.
doi: 10.36922/ijb.1673

Received: August 24, 2023
Accepted: November 21, 2023
Published Online: January 18, 2024

1. Introduction

Ovarian cancer is the most fatal gynecological malignancy with a high mortality/morbidity ratio primarily attributed to the lack of specific symptoms and effective early screening strategies.[1] Despite advances in cancer treatment, survival rates for ovarian cancer have remained largely unchanged, even in medically advanced countries such as the United States and Canada, where only about 47% of patients survive five years after diagnosis.[2] Currently, cytoreductive surgery and cisplatin-based chemotherapy remain the preferred treatment options,[3,4] while the continuous development and updates in immunotherapy, targeted therapy, and combinatorial chemotherapy offer

new opportunities for clinical treatment.[5] Nevertheless, the efficacy of these treatments varies considerably among patients with ovarian cancer. This can be partly ascribed to the heterogeneity of individual tumors. As a matter of fact, personalized precision therapy for patients holds promise for improving overall survival rates.[6]

In recent years, the rapid advancement of 3D bioprinting technology has created a powerful platform for achieving patient-specific precision therapy. In contrast to other common 3D culture methods such as organoids and patient-derived xenografts, 3D bioprinting is extensively utilized in the development of functional tissues and organs,[7-10] construction of *in vitro* tumor models,[11-13] screening of anti-tumor drugs[14-16] and oncotherapy,[17] owing to its simplicity, low cost, and high stability. In addition, traditional screening tools for anti-tumor drugs are typically focused on two-dimensional planar cultures, which lack the inherent characteristics of the 3D environment *in vivo*, such as cell-cell interactions and cell-matrix interactions.[18,19] Therefore, 2D models may produce inaccurate results in the screening of anti-tumor drugs. In our previous study, we successfully created *in vitro* tumor models of hepatocellular carcinoma and cholangiocarcinoma using 3D bioprinting technology and assessed the effectiveness of anti-tumor drugs.[20-22] More importantly, a growing body of research confirms that 3D bioprinting technology is undoubtedly a promising approach to produce *in vitro* cancer model, thus allowing identification of patient-specific sensitive drugs.[23-25]

As previously described, the tumor microenvironment (TME) is a complex ecosystem that supports cancer initiation, progression, and invasion.[26] Undoubtedly, the ovarian cancer microenvironment is a crucial factor affecting the overall and progression-free survival of patients with ovarian cancer.[27,28] To be specific, the components of the TME, including the neighboring stromal cells and the extracellular matrix (ECM) secreted by tumors, interact with tumor cells in a complex and multifaceted manner to regulate chemotherapy resistance.[29-31] There is growing evidence that the biophysical properties of TME, such as stiffness, have implications for gene expression and behaviors of tumor cells. For instance, Wei *et al.* quantitatively confirmed that omental metastases are rich in desmoplasia and stiffer than paired primary tumors, and further demonstrated that matrix rigidity can modulate ovarian cancer progression.[32] Additionally, an interesting study by Kim *et al.* described a mechanically enhanced bioink that mimics the biochemical microenvironment characteristics of gastric cancer and exhibits more aggressive cancer-related traits, such as cell aggregation, cell interactions, and drug resistance.[33] Moreover, Tang *et al.* employed rapid 3D bioprinting to create multizone glioblastoma models with different stiffness, revealing that a rigid ECM microenvironment induces mesenchymal phenotypes that are linked to patient recurrence and unfavorable treatment results.[34] Another study conducted by Yang *et al.* identified many stiffness-sensing genes and genes enriched in cancer-related pathways by RNA-seq analysis of ovarian cancer cells grown in matrix of different stiffness, confirming that ovarian cancer is a mechanically responsive tumor.[35] At the same time, Pietilä *et al.* found that matrix hardness altered ECM signaling in high-grade serous cancer (HGSC) cells and that increased ECM stiffness protected HGSC cells from cisplatin therapy.[36] While these studies provide insights into matrix stiffness and tumor biological behavior, the approaches to model tumors with different levels of stiffness described above are complicated. Consequently, a simple and high-efficiency modeling method is urgently needed to simulate ovarian cancer tissues with various rigidity.

In this study, we fabricated *in vitro* models of ovarian cancer with various levels of stiffness in a more efficient and flexible way using 3D bioprinting technology. By modifying the hydrogel concentration, we simulated ovarian cancer tissues with various levels of stiffness and investigated the potential impact of ECM rigidity on pharmacodynamics. Accordingly, our study may provide practical guidance for oncologists to adjust drug regimens appropriately according to the stiffness of tumor tissue. In addition, we proved that 3D bioprinting technology is also an effective technique paving the way for investigating the correlation between tumor stiffness and biological activity, facilitating further exploration of disease mechanisms and new drugs.

2. Materials and methods

2.1. Cell culture

Human ovarian cancer cell line SKOV3 was purchased from Procell Life Science & Technology Co., Ltd. (Wuhan, Hubei, China). The cells were cultured in SKOV3 cell-specific medium (ProCell, Wuhan, China). Cells were cultured in a 5% CO_2 incubator at 37°C and passaged using trypsin (0.25%; Invitrogen, Carlsbad, USA) after reaching ~80% confluence. The culture medium was replaced every two days.

2.2. Rheological measurements

Rheological measurements were performed using a Physica MCR 302 rheometer (Anton Paar, Germany) with a cone-plate geometry measuring system (25 mm diameter, 2° cone angle, 99 truncation gap). The storage modulus (G') and loss modulus (G'') were recorded as a function of time through oscillatory measurements under a strain of 0.1% and frequency of 1.5 Hz. Besides that, temperature sweep

oscillatory tests were also conducted through cooling process with the rate of 5°C/min. The intersection of the G' and G'' curves is generally considered the gel point of the material. Different concentrations (6% and 8%) of GelMA were incubated at 37°C before testing and the temperature-controlled testing plate was also set at 37°C as the initial temperature. The time dependence of G' and G'' of GelMA hydrogels with different concentrations were measured according to a set measurement temperature (21.5°C), which corresponded to the setting of the printing temperature.

2.3. Semi-quantification of printability

When GelMA is in the ideal gelation state, the extruded filaments will show a clear morphology, marked by regular grids and square holes in the manufactured structure. We utilized the following formula to calculate GelMA printability (Pr) based on the square shape:[37]

$$\mathrm{Pr}=\frac{L^2}{16A} \quad \text{(I)}$$

where L means perimeter, and A means area. For an acceptable printability state, the interconnected channels of the 3D-bioprinted model would be square shape, and the Pr value was 1. To determine the Pr value of each concentration of GelMA at printing temperature, optical images of printed models were analyzed in ImageJ software (version 1.8.0) to calculate the perimeter and area of interconnected channels (n = 4).

2.4. Construction of 3D-bioprinted ovarian cancer model

A 3D cellular bioprinter BIOMAKER (SUNP Biotech, Beijing, China) was used to construct *in vitro* ovarian cancer models according to previously reported procedures.[22,23,38] Briefly, 10% gelatin methacryloyl (GelMA) hydrogels (EFL-GM-30, Engineering for Life, China) were prepared with phosphate-buffered saline (PBS) containing 0.25% (w/v) lithium phenyl(2,4,6-trimethylbenzoyl) phosphinate (EFL-GM-30, Engineering for Life, China). SKOV3 cells cultured in a 2D environment were collected and prepared as a suspension. The cell suspension was then mixed with 10% GelMA in a volume ratio of 2:3 (6%-3DP) or 1:4 (8%-3DP), with a final cell density of 5×10^6/mL. The cell/hydrogel mixture was pumped into a sterile syringe with a 23G needle and placed in a 3D bioprinter at a controlled temperature. The temperature of nozzle and molding chamber was 21.5°C and 10°C, respectively. The cell/hydrogel mixture was squeezed at a rate of 1 mm^3/s to fabricate the model and then exposed to a blue laser (wavelength 405 nm) for 20 s to modify the GelMA. Afterward, 1 mL SKOV3 cell-specific medium was added to each well of the 24-well plate. The culture medium was changed every two days.

2.5. Young's modulus tests

For each concentration of samples, the same 3D bioprinter was used to construct cuboids, which were 2 cm long, 1 cm wide and 0.6 cm high. Young's modulus tests were also performed on 3D models containing 6% GelMA and 8% GelMA but without tumor cells, in addition to 3D tumor models. Prior to the determination of Young's modulus, all samples were measured with vernier caliper to determine their actual sizes, including length, width, and height. Three samples of each condition were loaded and compressed until rupture at the rate of 0.05 mm/s using a mechanical test instrument (Bose ElectroForce 3200, Bose Corp.). The elastic part (10% to 20% strain) of the stress-strain curve was used to calculate the Young's modulus.

2.6. Cell survival assay

Cell survival in the 3D-bioprinted models was assessed on days 1, 3, 5, 7, and 10 after printing. Cell survival was measured using a live/dead fluorescence assay. Briefly, a mixture of calcein-AM (C-AM, 1 μmol/L; Sigma-Aldrich, Burlington, USA) and propidium iodide (PI, 2 μmol/L; Sigma-Aldrich, Burlington, USA) was prepared and passed through a 0.22-μm filter prior to staining. The 3D-bioprinted model was gently washed with PBS and incubated in a C-AM/PI mixture at 37°C for 30 minutes in the dark. After incubation, the 3D-bioprinted model was gently washed with PBS and observed using a laser-scanning confocal microscope (C2/C2si; Nikon, Tokyo, Japan). Five random fields were captured for each sample, and the cells in the five samples were counted using the ImageJ software (Version 1.8.0). Cell survival (%) was calculated using the following formula:

$$Cell\,survival(\%)=\frac{Number\,of\,live\,cells}{Total\,number\,of\,cells}\times100 \quad \text{(II)}$$

2.7. Cell proliferation assay

The 2D-Ov cells and 3D-bioprinted cells on days 1, 3, 5, 7,10 after printing were incubated in a mixture of culture medium and Cell Counting Kit 8 (CCK8; Dojindo, Kumamoto, Japan) at a volume ratio of 9:1. After 2 h of incubation at 37°C, the absorbance of the culture medium at 450/620 nm was measured (AMR-100; ALLSHENG, Hangzhou, China).

2.8. Evaluation of protein and mRNA expression

The expression of ovarian cancer-associated proteins and multidrug resistance genes was evaluated using several methods. Ki-67 and p53 protein expression were detected by immunofluorescence, and the mRNA expression of *p53*,

IL-6, *CD133*, *ALDH1*, *CD44*, *ABCA1*, *MRP-1*, and *MDR-1* was detected by real-time quantitative polymerase chain reaction. The antibody details and primer sequences are shown in Tables 1 and 2, respectively.

2.9. Pharmacodynamic evaluation of antitumor drugs

On day 7 after printing, 3D-bioprinted cells were treated with a range of concentrations of carboplatin (1 μM, 10μ M, 30 μM, 50 μM, 70 μM, 100 μM), paclitaxel (0.1 nM, 1 nM, 10 nM, 1000 nM, 50000 nM) and olaparib (1 μM, 10 μM, 30 μM, 50 μM, 100 μM, 150 μM). When 2D-Ov cells reached approximately 70–80% confluence, they were treated with different concentrations of the antitumor drugs listed above. Cell growth was measured using the CCK8 assay, and dose-response curves were plotted using GraphPad Prism (Version 9.0.0, San Diego, CA, USA).

2.10. RNA sequencing and bioinformation analysis

RNA was extracted using the TRIzol method (Invitrogen, CA, USA) and treated with RNase-free DNase I (Takara, Kusatsu, Japan). A total amount of 1.5 μg RNA per sample was used as input material for the RNA sample preparations. Sequencing libraries were generated using NEBNext® Ultra™ RNA Library Prep Kit for Illumina® (NEB, USA) following recommendations of manufacturer and index codes were added to attribute sequences to each sample. The library preparations were sequenced on an Illumina Novaseq 6000 platform by the Beijing Allwegene Technology Company Limited (Beijing, China), and paired-end 150 bp reads were generated. Differential expression analysis of two conditions/groups was performed using the DESeq R package (1.10.1). Genes with an adjusted *p*-value <0.05 found by DESeq were assigned as "differentially expressed." Gene Ontology (GO) enrichment analyses of differentially expressed genes (DEGs) were implemented using the cluster Profiler R package. GO terms with corrected p <0.05 were considered significantly enriched by DEGs.

2.11. Statistical analysis

Data are expressed as mean ± standard deviation. Student's *t*-test was used to determine whether there was a statistically significant difference between groups. Statistical significance was defined as $^{*}p$ <0.05, $^{**}p$ <0.01, $^{***}p$ <0.001, $^{****}p$ <0.0001.

3. Results

3.1. Rheological evaluation

For assessment of printability, we conducted rheological evaluation for two concentrations of GelMA. As shown in Figure 1A, temperature sweep oscillatory tests were performed through cooling process, the temperature to reach G' and G'' crossover of 6% GelMA and 8% GelMA were about 18.8°C and 20.7°C, respectively. When temperature is higher than crosslinking temperature, G'' is greater than G', and the GelMA hydrogels would be in a fluid or sol state. In addition, the results of time sweep tests demonstrated that the different concentrations of GelMA showed time-dependence properties when operating from

Table 1. Antibodies used in immunofluorescence experiment

Antibodies	Concentration	Source
Rabbit anti--human Ki-67	1:100	Abcam, Cambridge, UK
Mouse anti-human p53	1:100	Abcam, Cambridge, UK
Goat anti-Rabbit (Alexa Fluor® 594)	1:300	Abcam, Cambridge, UK
Goat anti-Mouse (Alexa Fluor® 488)	1:300	Abcam, Cambridge, UK

Table 2. Primers used in quantitative polymerase chain reaction (qPCR)

Gene	Forward (5'-3')	Reverse (5'-3')
p53	ACTTGTCGCTCTTGAAGCTAC	GATGCGGAGAATCTTTGGAACA
IL-6	GCCAGAGCTGTGCAGATGAG	CAGTGGACAGGTTTCTGACC
CD133	AGTCGGAAACTGGCAGATAGC	GGTAGTGTTGTACTGGGCCAAT
ALDH1	CCCTGGAGACGATGGATACAG	TCTGAGGGTTCTAATACAGCCC
CD44	CTGCCGCTTTGCAGGTGTA	CATTGTGGGCAAGGTGCTATT
ABCA1	TCTCACCACTTCGGTCTCCATG	CCTCGCCAAACCAGTAGGACTT
MRP-1	TCTACCTCCTGTGGCTGAATCTG	CCGATTGTCTTTGCTCTTCATG
MDR-1	TTGCTGCTTACATTCAGGTTTCA	AGCCTATCTCCTGTCGCATTA
GAPDH	CGAGATCCCTCCAAAATCAA	TTCACACCCATGACGAACAT

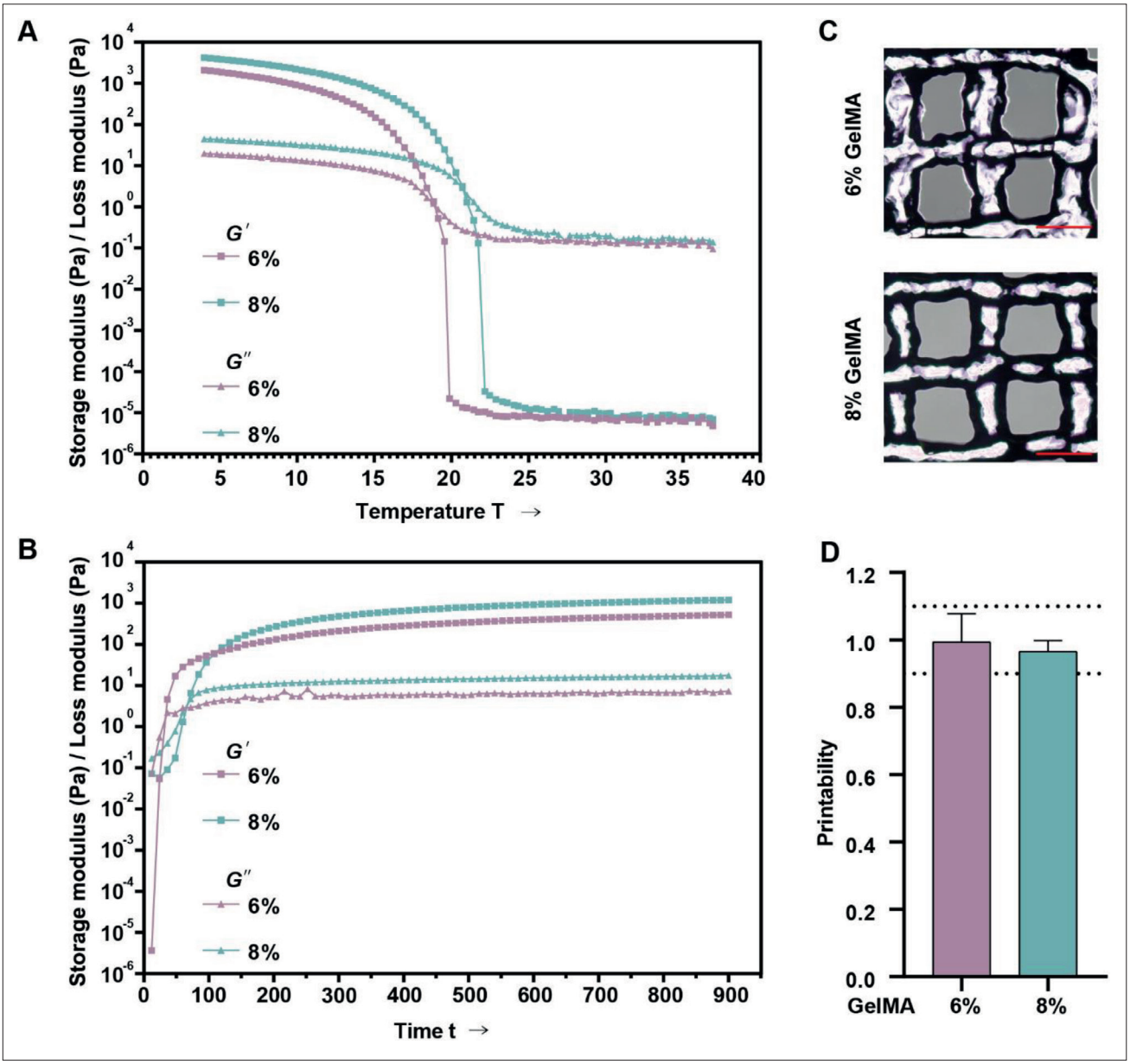

Figure 1. Rheological measurement and Young's modulus for different 3D-bioprinted models. (A) Temperature sweep tests showing storage modulus (G') and loss modulus (G'') with cooling rate of 5°C/min for 6% GelMA and 8% GelMA. (B) Time sweep tests showing G' and G'' under 21.5°C for 6% GelMA and 8% GelMA. (C) Optical images of 3D-printed models with different concentrations of GelMA. Scale bar: 500 μm. (D) Semi-quantitation of Pr values of 3D-printed models with different concentrations of GelMA.

initial temperature of 37°C to the measured temperature of 21.5°C. To be specific, 8% GelMA had a relatively higher modulus compared to 6% GelMA (Figure 1B). In our study, in order to evaluate the printability of bioinks semi-quantitatively, the Pr values of each concentration of GelMA were calculated by **Equation I**. According to previous study,[37] 3D-bioprinted models will exhibit satisfying morphology when Pr is in the range of 0.9 to 1.1. Figure 1D show that Pr values of 6% GelMA and 8% GelMA are 0.994±0.083 and 0.966±0.032, respectively.

3.2. Construction of 3D-bioprinted ovarian cancer model

To simulate the TME *in vivo*, a 3D-bioprinted ovarian cancer tumor model with a lattice structure was constructed *in vitro* (Figure 2A). The 3D bioprinting technology allows for the quick generation of various fine structures with

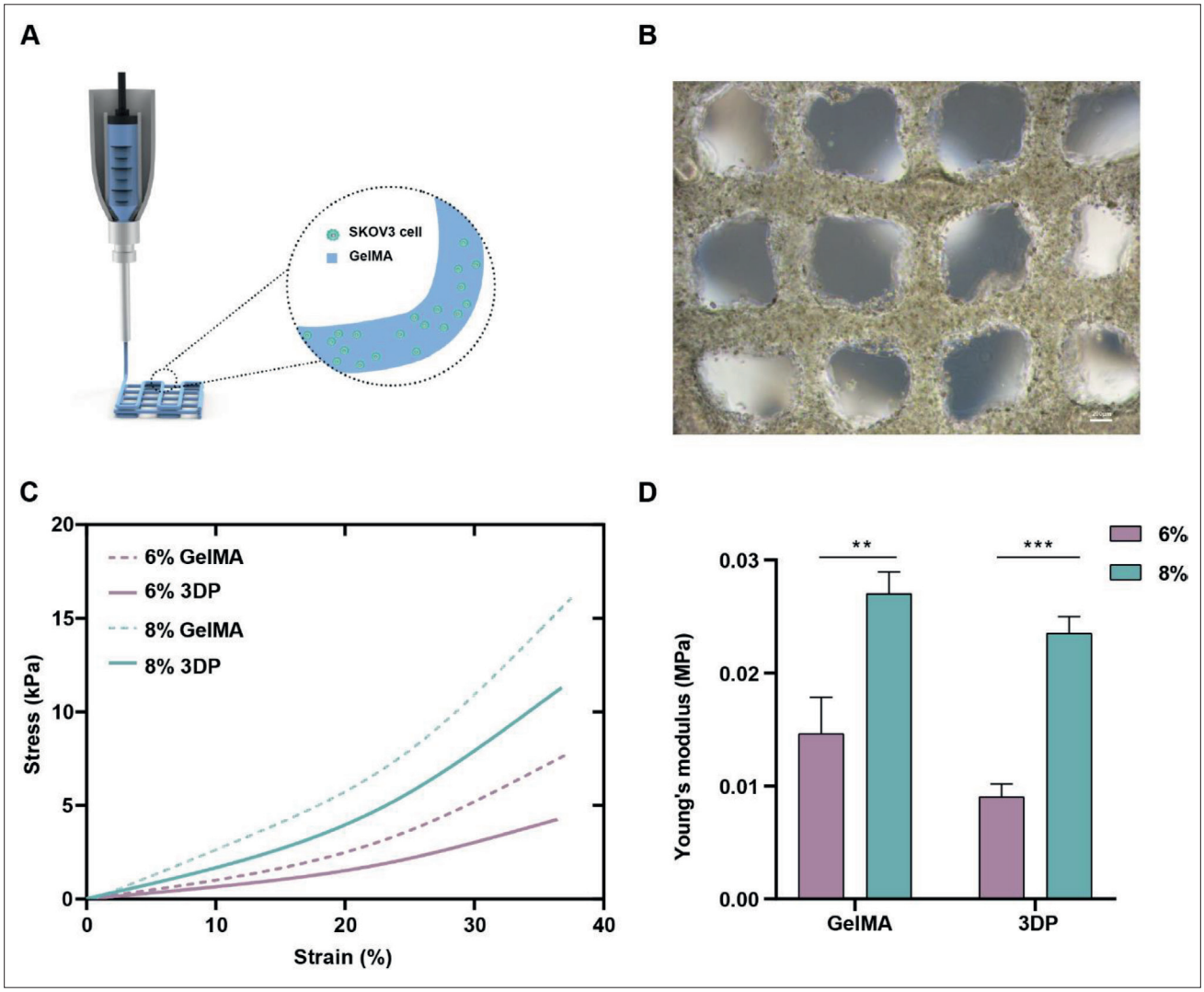

Figure 2. Fabrication of 3D-bioprinted ovarian cancer model. (A) Schematic illustration of the 3D bioprinting process. (B) An image of the 3DP-Ov model. Scale bar: 200 μm. (C) Representative stress-strain curves of 3D models under different conditions. (D) Young's modulus of 3D models under different conditions.

high resolution tailored for research purposes. Figure 2B shows the resulting 3D-bioprinted ovarian cancer model. Our preliminary study involved exploring suitable bioink materials and 3D bioprinting technologies for cell growth and proliferation.[23] We used GelMA, a hydrogel containing ovarian cancer cells, to print a 3D lattice structure measuring 6 mm in length, 6 mm in width, and 1 mm in height, according to a preset procedure.

To investigate the impact of ECM stiffness on tumor cells, we mixed tumor cell suspensions with 10% GelMA hydrogel in suitable proportions to create tumor models with GelMA concentrations of 6% (*i.e.*, 6%-3DP) and 8% (*i.e.*, 8%-3DP). As presented in Figure 2C, stress-strain curves of 3D models under various conditions were obviously different. To be specific, the Young's moduli of 6%-3DP and 8%-3DP tumor models were 0.009±0.001 MPa and 0.024±0.001 MPa with a significant difference. Additionally, for the 3D-bioprinted models without tumor cells, the Young's modulus of 6% GelMA and 8% GelMA were 0.015±0.003 MPa and 0.027±0.002 MPa, respectively (Figure 2D).

The 3D-bioprinted ovarian cancer model was cultured in SKOV3 cell medium with medium changes every two days. C-AM/PI staining was used to evaluate the viability of tumor cells in 3D ovarian cancer model. The results revealed that cell viability of 6%-3DP was approximately 82% on the first day after printing. With the extension of culture time after printing, cell viability gradually increased

and remained stable at over 90% from the fifth day after printing (Figure 3A).

Compared to ovarian cancer cells grown under traditional 2D conditions (2D-Ov), tumor cells cultured under 3D conditions exhibited strong proliferative capability. Specifically, the growth rate of 6%-3DP cells was lower on the first to third day. However, on day 4, the cell proliferation rates in both cultures became equal.

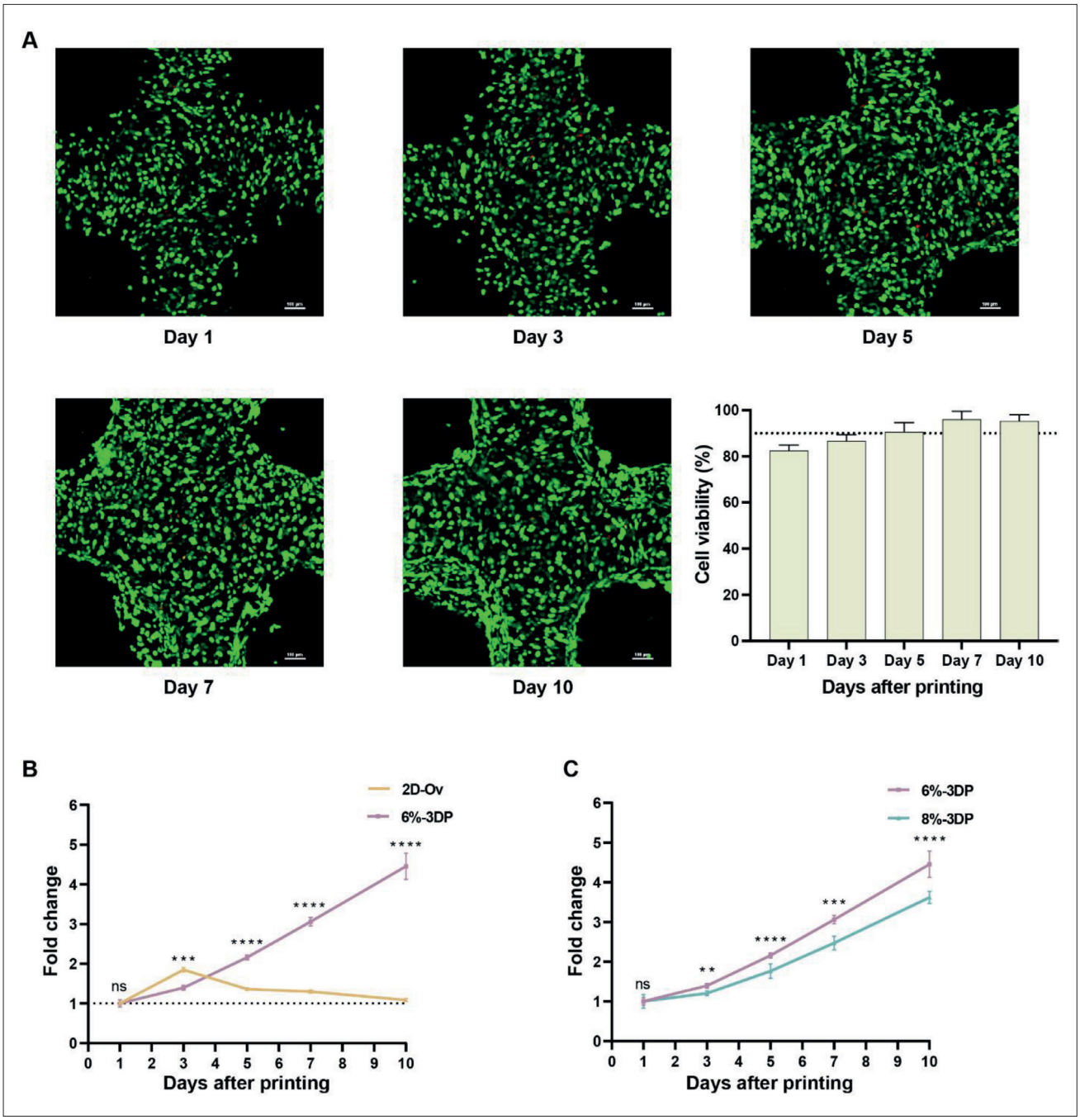

Figure 3. Cell survival and proliferation in 3D-bioprinted ovarian cancer model. (A) Representative live-dead staining images of 6%-3DP model captured on days 1, 3, 5, 7, and 10, and cell viability of 6%-3DP model at different time points after printing. Live and dead cells were labeled with calcein-AM (green) and PI (red), respectively. Scale bar: 500 μm. (B) Proliferation rates of 2D-Ov and 6%-3DP cells at different time points after printing. (C) Proliferation rates of 6%-3DP and 8%-3DP cells at different time points after printing. The results are expressed as fold change compared to day 1. ns, not significant; $^{**}p$ <0.01; $^{***}p$ <0.001; $^{****}p$ <0.0001.

Since then, the 6%-3DP model maintained a high growth rate, while because there was not enough room to grow, the number of cells in the 2D model gradually decreases. Moreover, the amount of cells in the 6%-3DP model increased approximately four times by day 10, while the number of cells on day 10 in the 2D model was similar to that on day 1 (Figure 3B). Notably, in both 3D models, the cells maintained a high growth rate. Nevertheless, differences in the rate of proliferation between the two models began to appear starting day 3, and by day 10, the number of cells in the 6%-3DP and 8%-3DP models had approximately quadrupled and tripled, respectively, as compared to the cell number on day 1 (Figure 3C).

3.3. Tumor-related protein and mRNA expression

To assess the biological activity of tumor cells in the 3D-bioprinted models, we used immunofluorescence to detect the expression of ovarian cancer-related proteins in 6%-3DP and 8%-3DP models. Our findings revealed that Ki-67 and p53 proteins were expressed in both models, indicating high activity of tumor cells in these models (Figure 4).

To investigate whether ECM stiffness affects tumor-related genes, we extracted mRNA from cells in 6%-3DP and 8%-3DP models 10 days after printing. We evaluated the expression of *p53*, *IL-6*, *ALDH1*, *CD44* and *CD133* genes. Our findings indicate that the levels of *p53* and *IL-6* mRNA were approximately eight- and three-fold higher, respectively, in 8%-3DP group than in 6%-3DP group. Additionally, as the stiffness of 3D tumor model increased, the expression of tumor stemness markers ALDH1 and CD44 was upregulated, whereas the expression of CD133 did not change significantly (Figure 5).

3.4. Effects of antitumor drugs on 2D-Ov and 3D-bioprinted model

Initially, we evaluated the response of 2D-Ov and 6%-3DP cells to anti-tumor drugs by treating both models with carboplatin, paclitaxel, and olaparib for 72 h. Our results revealed that the IC_{50} values of carboplatin, paclitaxel, and olaparib in the 6%-3DP models were significantly higher compared to those in 2D-Ov models (62.85 vs. 9.921 μM, 3.305 vs. 0.004 μM, 27.17 vs. 8.119 μM, respectively) (Figure 6).

3.5. Effects of antitumor drugs on 3D-bioprinted models with different stiffness

To further investigate the impact of the structural stiffness of 3D tumor models on pharmacodynamics, we treated 6%-3DP and 8%-3DP models with carboplatin, paclitaxel, and olaparib for 72 h. Our findings indicated that the IC_{50} values of the three anti-tumor drugs measured in the 8%-3DP model were higher than those measured in the 6%-3DP model (127.6 vs. 62.85 μM, 4.997 vs. 3.305 μM, 39.59 vs. 27.17 μM, respectively) (Figure 7A–C).

To investigate the mechanism underlying the differences in the pharmacodynamics of 3D ovarian cancer models with different stiffness, we collected RNA from 6%-3DP and 8%-3DP cells after 10 days of culture and evaluated the expression of multidrug resistance genes. Our results revealed that the stiffness of ECM affects the expression of drug resistance genes. In 8%-3DP model, the expression of *MDR1* and *MRP1* genes were obviously increased, and their mRNA levels were approximately four and two times higher than those in 6%-3DP model, respectively. However, there was no significant difference in ABCA1 expression between the two groups (Figure 7D–F).

3.6. Transcriptional profiling of 3D-bioprinted models with different stiffness

Next, we found significant differences in transcriptional profile between the 6%-3DP and 8%-3DP models. A total of 217 DEGs were identified, including 145 upregulated genes and 72 downregulated genes (Figure 8A and 8B). To explore the functional characteristics of DEGs, we performed GO pathway enrichment analysis. GO analysis results demonstrated that the upregulated genes were obviously enriched in "metabolic process," "response to chemical," "phosphorus metabolic process," "response to organic substance," and "response to endogenous stimulus." For the downregulated DEGs, the most enriched GO terms included "immune system process," "interspecies interaction between organisms," "response to external stimulus," "regulation of response to stress," and "response to biotic stimulus" (Figure 9).

Additionally, bioinformatics analysis also revealed that elevating the stiffness of the 3D-bioprinted ovarian cancer model led to increased expression of key genes associated with chemotherapy resistance, namely *EGR1*, *FOS*, *CRYAB*, *G6PD*, *DUSP1*, *PIM1*, *PPDPF*, *HDAC5*, and *FGFR4* (Figure 8C). These findings align with previous research that has confirmed the correlation between overexpression of these genes and enhanced chemoresistance, which has implication on shortening the overall survival durations.[39-47]

4. Discussion

In this study, we used 3D bioprinting technology to construct *in vitro* ovarian cancer tumor models and generated ovarian cancer models with varying degrees of stiffness by adjusting GelMA hydrogel content. Thus, we were able to simulate ovarian cancer tissues with different levels of stiffness that closely resembled those observed in clinical settings. Compared with traditional 2D models,

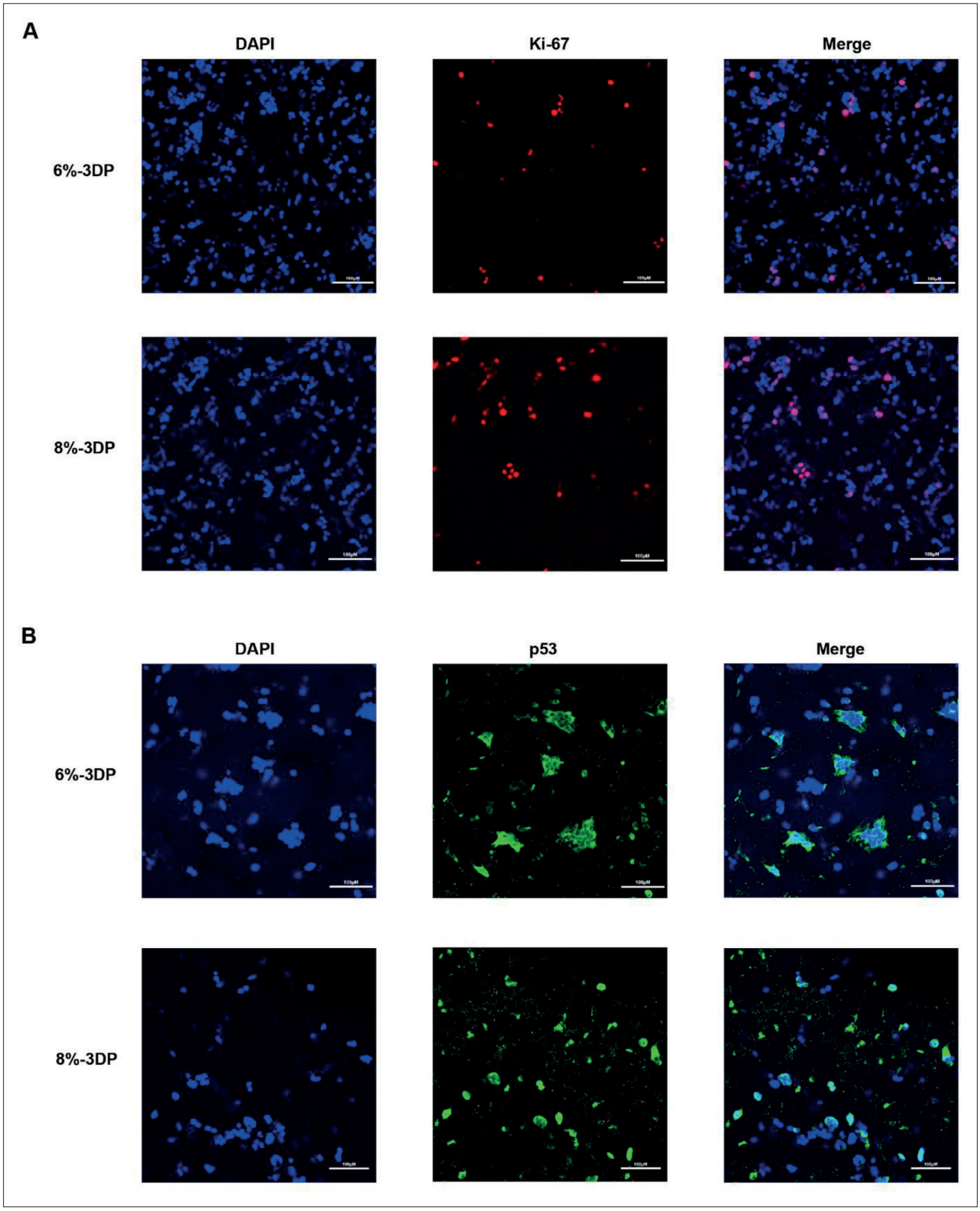

Figure 4. Ovarian cancer-related protein expression in 3D-bioprinted ovarian cancer models with different stiffness. (A) The expression of Ki-67 in 6%-3DP and 8%-3DP models. (B) The expression of p53 in 6%-3DP and 8%-3DP models.

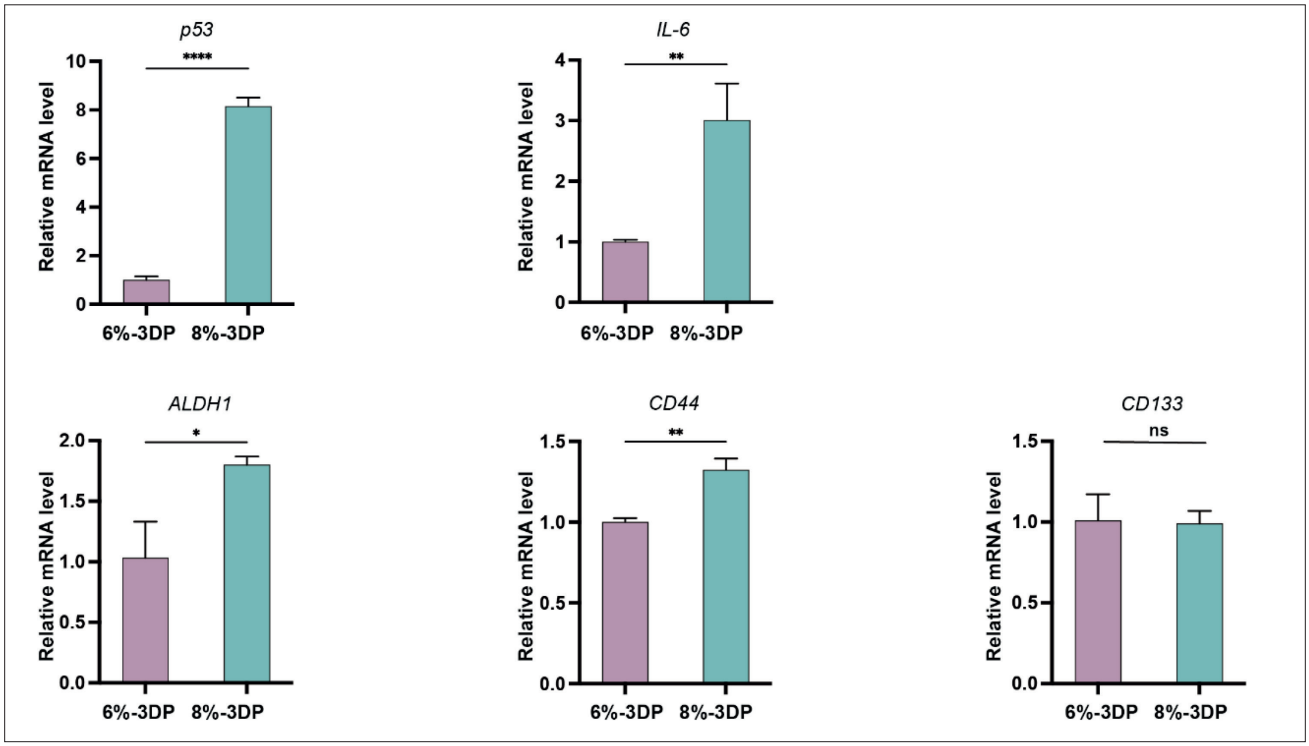

Figure 5. Ovarian cancer-related mRNA expression in 3D-bioprinted ovarian cancer models. The expression of tumor-related genes, including *p53*, *IL-6*, *ALDH1*, *CD44* and *CD133* in 6%-3DP and 8%-3DP models. ns, not significant; **p* <0.05; ***p* <0.01; *****p* <0.0001.

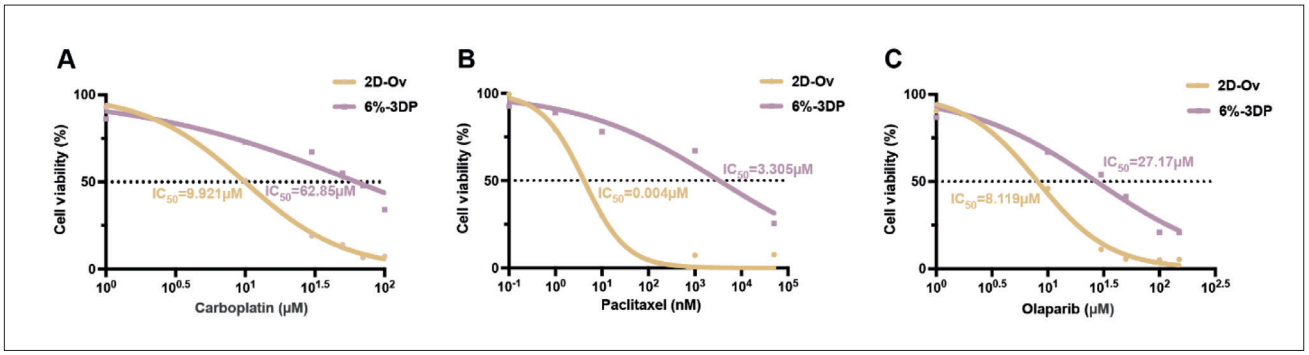

Figure 6. Characteristics of drug metabolism across various ovarian cancer models. Dose-effect curves of carboplatin (A), paclitaxel (B), and Olaparib (C) in the 2D-Ov and 6%-3DP models after 72 h of treatment.

3D models provide tumor cells in a microenvironment that bear greater resemblance to the one found *in vivo*, especially in the aspects of specific cell size, spatial distribution of cells, cell geometry, and ECM components.[48,49] These factors significantly affect the functional state of and interactions between tumor cells. Previous studies have shown that increased matrix stiffness can promote the malignant phenotype of tumors during progression.[50] Furthermore, evidence suggests that stiffness, an important characteristic of the ECM, can significantly influence cancer cell responses to treatment and chemotherapy resistance.[51] Consistent with these findings, we observed that increasing the stiffness of the tumor ECM reduced the sensitivity of tumor cells to antitumor drugs.

Three-dimensional tumor models, particularly those developed through 3D bioprinting, hold great promise for advancing next-generation precision therapies.[52] These models have garnered global support, and the most recent milestone was marked by the United States passing a law in December 2022 that enables new drugs to be approved by the U.S. Food and Drug Administration (FDA) without

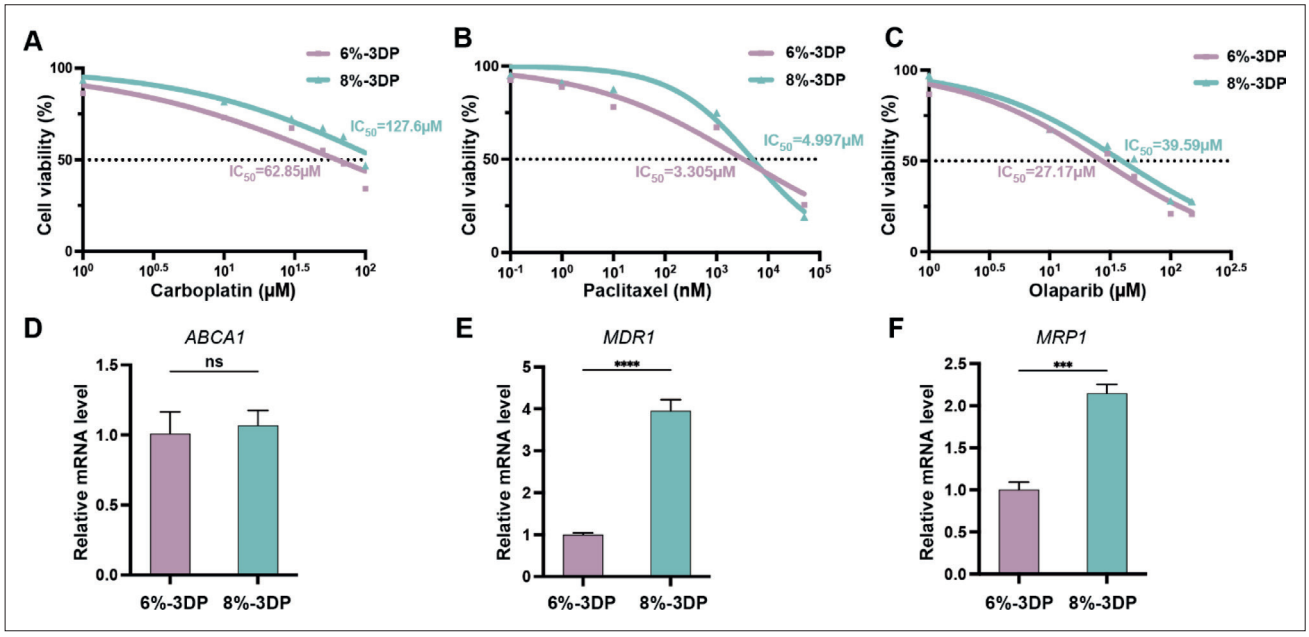

Figure 7. Profiles of drug metabolism of 3D-bioprinted ovarian cancer models with different stiffness. (A–C) Dose-effect curves of carboplatin (A), paclitaxel (B), and olaparib (C) in 6%-3DP and 8%-3DP models after 72 h of treatment. (D–F) mRNA expression of drug resistance genes, including *ABCA1* (D), *MDR1*(E), and *MRP1*(F) in 6%-3DP and 8%-3DP models. ns, not significant; ***p <0.001; ****p <0.0001.

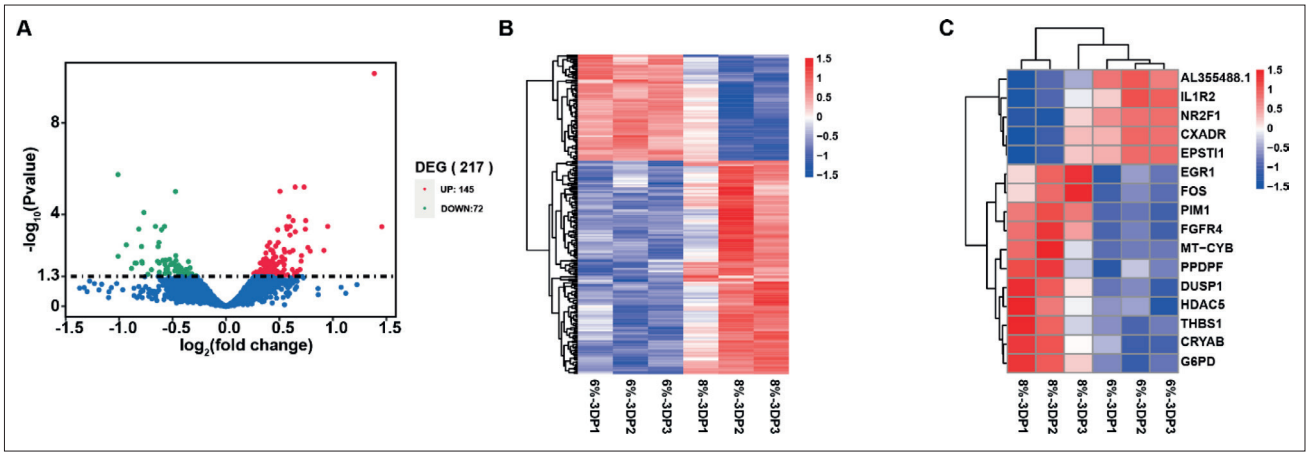

Figure 8. Transcriptional profiling of 3D-bioprinted ovarian cancer models with varying stiffness. (A) Volcano plot of 217 differentially expressed genes (DEGs), including 145 significantly upregulated DEGs (red spots) and 72 significantly downregulated DEGs (green spots). (B) Cluster analysis of DEGs of the 6%-3DP and 8%-3DP models. Rows represent genes, and columns represent samples. (C) The heatmap of 16 significantly DEGs. Red represents upregulated genes, and green represents downregulated genes.

requiring animal testing. This legislation also permits the FDA to progress from drug or biological testing to human testing after conducting non-animal testing. An increasing number of researchers have recognized the value of non-animal methods such as computer modeling and organ chips in drug testing and development. 3D bioprinting offers a unique opportunity to test novel drugs that currently lack clinical data. As a result, tumor models constructed *in vitro* using 3D bioprinting technology can facilitate preclinical prediction, which conforms to the new trend of tumor research in the era of precision medicine.

Our team constructed an ovarian cancer tumor model using straightforward, time-saving, and economical extrusion-based bioprinting techniques. The tumor model demonstrated structural stability in culture post-printing, maintained high cell vitality and proliferation

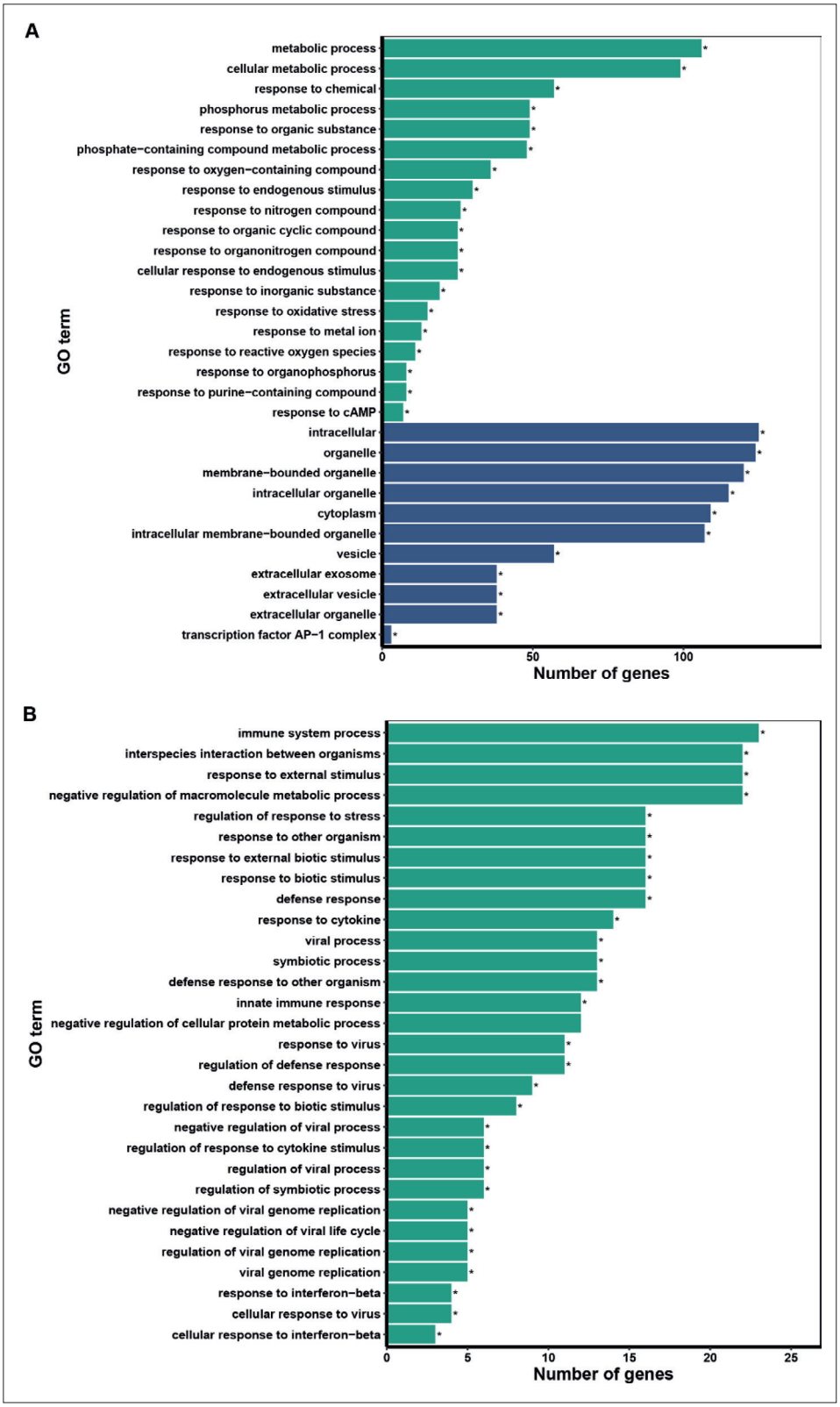

Figure 9. GO enrichment analysis of differentially expressed genes (DEGs) in 3D-bioprinted ovarian cancer models with varying stiffness. (A) Gene Ontology (GO) enrichment analysis of upregulated genes. (B) GO enrichment analysis of downregulated genes. Green color indicates biological process, and blue color indicates cellular component.

ability, and provided a solid foundation for later-stage pharmacodynamic research on antitumor drugs. In addition to extrusion-based bioprinting, other 3D culture methods, such as organoids and patient-derived xenografts (PDXs), are gaining attention. Despite the utilization of organoids in studying various diseases, including cancer, the cost factor and a lack of standardization in terms of establishment and quality control are still a matter of concern.[53] On the other hand, PDXs belong to a type of tumor tissue that is extracted from biopsies or surgical excisions and propagated in mice via implants and explants.[54] To some extent, the propagation of this tissue via culturing method can still accurately retain the genomic and transcriptomic characteristics of the parental tumor tissue, and the resultant cultures can be used for measuring tumor response to treatment; however, it has several shortcomings, such as the time-consuming and costly culturing process, and the likelihood of intratumoral heterogeneity and genome evolution. Additionally, the existing PDX models, which are constructed with tissues acquired from immunodeficient mice, are not feasible for use in immuno-oncology research.[55] Therefore, the development of new 3D tumor models for preclinical studies is imperative.

Before the construction of 3D tumor models, we first performed rheological analysis for both concentrations of GelMA hydrogels. Temperature sweep oscillatory tests indicated that the temperature at which 6% GelMA and 8% GelMA reached the intersection of G' and G'' was about 18.8°C and 20.7°C, respectively. Therefore, in the subsequent experiments, we set the printing temperature at 21.5°C to avoid extrusion needle clogging, to reduce the damage of shear stress on tumor cells during the printing process and ensure good formability of printed structure. Furthermore, the results of semi-quantification of printability showed that the Pr values of 6% GelMA and 8% GelMA were both close to 1. As a result, smooth and uniform filaments could be continuously extruded, resulting in a standard grid structure with obvious layering.

When examining the biological behavior of tumor cells in 3D tumor models, we observed that 8%-3DP model exhibited a lower rate of cell proliferation than 6%-3DP model. However, we also noted a higher expression level of p53, an ovarian cancer cell marker, in 8%-3DP model. Additionally, increasing the stiffness of the tumor model resulted in a significant increase in the expression levels of the tumor stemness markers like ALDH1[56] and CD44,[57] whereas the level of CD133[58] remained unchanged. Notably, the rigid model also showed higher expression levels of IL-6, a factor associated with poor prognosis and chemotherapy resistance in patients with ovarian cancer.[59] These findings suggest that appropriately increasing the stiffness of 3D tumor models may promote malignant phenotypes such as tumor stemness and tumor progression.

In pharmacodynamic research, it is widely accepted that pharmacodynamic results obtained from 3D culture conditions are more reliable than those obtained from 2D planar cultures. Our findings demonstrate that cell proliferation in 3D model (6%-3DP) was higher than that in 2D model. Furthermore, the IC_{50} values obtained using 3D model (6%-3DP) were more closely aligned with the clinically effective blood concentrations. Additionally, the responses of the two tumor models with different matrix stiffness to antitumor drugs also varied, with the IC_{50} values of the three tested drugs in 8%-3DP model being notably higher than those in 6%-3DP model. The expression of several common drug resistance genes, such as *MDR1* and *MRP1*, except for *ABCA1*, was upregulated in rigid model, partly accounting for the distinct responses of the two tumor models to the three tested chemotherapy drugs. Hence, 3D models offer a superior platform for preclinical drug testing, and matrix stiffness plays a critical role in modulating the sensitivity of tumor cells to chemotherapy drugs.

We also identified unique transcriptomic characteristics in the stiffer 3D-bioprinted ovarian cancer model. Specifically, 3D models with different levels of stiffness were found to manifest varied transcriptional expression profiles. In comparison to the 6%-3DP model, the 8%-3DP model showed elevated expression of 145 genes and attenuated expression of 72 genes. Notably, among these DEGs, we discovered several significant ones associated with enhanced chemotherapy resistance, including *FOS*, *CRYAB*, *G6PD*, and *DUSP1*. According to Javellana *et al.*, *FOS* was particularly upregulated in chemotherapy-resistant specimens obtained from a cohort of patients with advanced stage IIIC or IV high-grade serous ovarian cancer.[40] Another research confirmed that *CRYAB* overexpression was associated with acquired drug tolerance and poor patient prognosis.[41] Through a correlation analysis between chemoresistance data and gene expression profiles of ovarian cancer patient-derived spheroids, Yamawaki *et al.* proved that cisplatin resistance was significantly related with increased expression levels of *G6PD*.[42] In addition, Kang *et al.* demonstrated that *DUSP1* overexpression impaired chemotherapy response in ovarian cancer, whereas silencing the gene *in vivo* significantly enhanced sensitivity to paclitaxel and increased apoptosis.[43] Consistent with these findings, our study revealed that an increase in ECM stiffness can promote the expression of related genes, which collectively contributes to enhanced chemoresistance.

However, several limitations of this study need to be addressed. The TME is composed of various cellular

and noncellular components that drive tumor growth, invasion, metastasis, and response to therapy in a concerted manner.[31] Instead of using the typical set of ingredients including fibroblasts, endothelial cells, immune cells, *etc.*, we only utilized tumor cells, which constitute only part of the actual tumor environment in the human body, in this study. Secondly, the application of cell lines in preclinical studies suffer from several shortcomings, including reduced heterogeneity, potential of gene modification, and faster growth rates, as compared to primary tumors.[60] Therefore, tumor specimens obtained from surgical resection should be used to extract primary tumor cells, which are then printed into 3D tumor models for the investigations of mechanisms underlying tumor development and the individualized drug screening. Tumor models fabricated from actual human tissues allow for more realistic analysis of the correlation between primary tumor stiffness and drug sensitivity.

5. Conclusion

In conclusion, compared to traditional planar cultures, 3D tumor models have significant advantages in providing accurate preclinical drug testing results. Having biophysical characteristics, such as stiffness, equivalent to those of the natural TME, 3D *in vitro* tumor model holds promise as a more efficient and powerful platform for drug research.

Acknowledgments

None.

Funding

This work was supported by the National Natural Science Foundation of China (Grant No. 32271470), National High Level Hospital Clinical Research Funding (2022-PUMCH-C-045), Beijing Natural Science Foundation (7212077), and CAMS Innovation Fund for Medical Sciences (CIFMS) (No.2021-I2M-1-058).

Conflict of interest

The authors declare that the research was carried out without any commercial or financial relationships that could be perceived as a potential conflict of interest.

Author contributions

Conceptualization: Ying Shan, Yilei Mao, Ying Jin, Huayu Yang
Formal analysis: Liqian Wang, Ruiyi Yan
Funding acquisition: Yilei Mao, Huayu Yang
Investigation: Ying Shan, Mingchang Pang
Methodology: Ying Shan, Mingchang Pang, Liqian Wang, Yixin Mao, Chang Zhou, Jingyuan Ji
Resources: Yilei Mao
Supervision: Huayu Yang
Writing–original draft: Ying Shan, Mingchang Pang, Chang Zhou, Yixin Mao
Writing–review & editing: Huayu Yang
All authors participated in the research and approved the final version of the article.

Ethics approval and consent to participate

Not applicable.

Consent for publication

Not applicable.

Availability of data

Data used in this work are available from the corresponding authors upon reasonable request.

References

1. Alkmin, S., Patankar, M. S. & Campagnola, P. J., 2022, Assessing the roles of collagen fiber morphology and matrix stiffness on ovarian cancer cell migration dynamics using multiphoton fabricated orthogonal image-based models. *Acta Biomater*, 153:342-354.
doi: 10.1016/j.actbio.2022.09.037

2. Lheureux, S., Braunstein, M. & Oza, A. M., 2019, Epithelial ovarian cancer: Evolution of management in the era of precision medicine. *CA Cancer J Clin*, 69(4):280-304.
doi: 10.3322/caac.21559

3. Vescarelli, E., Gerini, G., Megiorni, F. *et al.*, 2020, MiR-200c sensitizes Olaparib-resistant ovarian cancer cells by targeting Neuropilin 1. *J Exp Clin Cancer Res*, 39(1):3.
doi: 10.1186/s13046-019-1490-7

4. Wang, M., Zhou, J., Zhang, L. *et al.*, 2019, Surgical treatment of ovarian cancer liver metastasis. *Hepatobiliary Surg Nutr*, 8(2):129-137.
doi: 10.21037/hbsn.2018.12.06

5. Herrera, F. G., Irving, M., Kandalaft, L. E. *et al.*, 2019, Rational combinations of immunotherapy with radiotherapy in ovarian cancer. *Lancet Oncol*, 20(8):e417-e433.
doi: 10.1016/s1470-2045(19)30401-2

6. Raghavan, S., Mehta, P., Ward, M. R. *et al.*, 2017, Personalized Medicine-Based Approach to Model Patterns of Chemoresistance and Tumor Recurrence Using Ovarian Cancer Stem Cell Spheroids. *Clin Cancer Res*, 23(22): 6934-6945.
doi: 10.1158/1078-0432.CCR-17-0133

7. Lee, A., Hudson, A. R., Shiwarski, D. J. *et al.*, 2019, 3D bioprinting of collagen to rebuild components of the human heart. *SCIENCE*, 365(6452):482-487.
doi: 10.1126/science.aav9051

8. Lee, S., Sani, E. S., Spencer, A. R. *et al.*, 2020, Human-Recombinant-Elastin-Based Bioinks for 3D Bioprinting of Vascularized Soft Tissues. *Adv Mater*, 32(45):e2003915. doi: 10.1002/adma.202003915

9. Li, C., Jiang, Z. & Yang, H., 2022, Advances in 3D bioprinting technology for liver regeneration. *Hepatobiliary Surg Nutr*, 11(6):917-919. doi: 10.21037/hbsn-22-531

10. Zhang, J., Yang, H. & Yang, H., 2022, Highlights of constructing liver-relevant in vitro models with 3D bioprinting. *Hepatobiliary Surg Nutr*, 11(6):896-898. doi: 10.21037/hbsn-22-486

11. Neufeld, L., Yeini, E., Pozzi, S. *et al.*, 2022, 3D bioprinted cancer models: from basic biology to drug development. *Nat Rev Cancer*, 22(12):679-692. doi: 10.1038/s41568-022-00514-w

12. Tang, M., Xie, Q., Gimple, R. C. *et al.*, 2020, Three-dimensional bioprinted glioblastoma microenvironments model cellular dependencies and immune interactions. *Cell Res*, 30(10):833-853. doi: 10.1038/s41422-020-0338-1

13. Park, W., Bae, M., Hwang, M. *et al.*, 2021, 3D Cell-Printed Hypoxic Cancer-on-a-Chip for Recapitulating Pathologic Progression of Solid Cancer. *J Vis Exp,* (167). doi: 10.3791/61945

14. Hong, S. & Song, J. M., 2022, 3D bioprinted drug-resistant breast cancer spheroids for quantitative in situ evaluation of drug resistance. *Acta Biomater*, 138:228-239. doi: 10.1016/j.actbio.2021.10.031

15. Mei, Y., He, C., Gao, C. *et al.*, 2021, 3D-Printed Degradable Anti-Tumor Scaffolds for Controllable Drug Delivery. *Int J Bioprint*, 7(4):418. doi: 10.18063/ijb.v7i4.418

16. Yi, H. G., Jeong, Y. H., Kim, Y. *et al.*, 2019, A bioprinted human-glioblastoma-on-a-chip for the identification of patient-specific responses to chemoradiotherapy. *Nat Biomed Eng*, 3(7):509-519. doi: 10.1038/s41551-019-0363-x

17. Shim, I. K., Yi, H. J., Yi, H. G. *et al.*, 2017, Locally-applied 5-fluorouracil-loaded slow-release patch prevents pancreatic cancer growth in an orthotopic mouse model. *Oncotarget*, 8(25):40140-40151. doi: 10.18632/oncotarget.17370

18. Hirschhaeuser, F., Menne, H., Dittfeld, C. *et al.*, 2010, Multicellular tumor spheroids: an underestimated tool is catching up again. *J Biotechnol*, 148(1):3-15. doi: 10.1016/j.jbiotec.2010.01.012

19. Abhinand, C. S., Raju, R., Soumya, S. J. *et al.*, 2016, VEGF-A/VEGFR2 signaling network in endothelial cells relevant to angiogenesis. *J Cell Commun Signal*, 10(4):347-354. doi: 10.1007/s12079-016-0352-8

20. Sun, L., Yang, H., Wang, Y. *et al.*, 2020, Application of a 3D Bioprinted Hepatocellular Carcinoma Cell Model in Antitumor Drug Research. *Front Oncol*, 10:878. doi: 10.3389/fonc.2020.00878

21. Mao, S., He, J., Zhao, Y. *et al.*, 2020, Bioprinting of patient-derived in vitro intrahepatic cholangiocarcinoma tumor model: establishment, evaluation and anti-cancer drug testing. *Biofabrication*, 12(4):045014. doi: 10.1088/1758-5090/aba0c3

22. Xie, F., Sun, L., Pang, Y. *et al.*, 2021, Three-dimensional bio-printing of primary human hepatocellular carcinoma for personalized medicine. *BIOMATERIALS*, 265:120416. doi: 10.1016/j.biomaterials.2020.120416

23. Yang, H., Sun, L., Pang, Y. *et al.*, 2021, Three-dimensional bioprinted hepatorganoids prolong survival of mice with liver failure. *GUT*, 70(3):567-574. doi: 10.1136/gutjnl-2019-319960

24. Tebon, P. J., Wang, B., Markowitz, A. L. *et al.*, 2023, Drug screening at single-organoid resolution via bioprinting and interferometry. *Nat Commun*, 14(1):3168. doi: 10.1038/s41467-023-38832-8

25. Mazzocchi, A., Soker, S. & Skardal, A., 2019, 3D bioprinting for high-throughput screening: Drug screening, disease modeling, and precision medicine applications. *Appl Phys Rev*, 6(1). doi: 10.1063/1.5056188

26. Wang, M., Zhao, J., Zhang, L. *et al.*, 2017, Role of tumor microenvironment in tumorigenesis. *J Cancer*, 8(5):761-773. doi: 10.7150/jca.17648

27. Yang, M., Lu, J., Zhang, G. *et al.*, 2021, CXCL13 shapes immunoactive tumor microenvironment and enhances the efficacy of PD-1 checkpoint blockade in high-grade serous ovarian cancer. *J Immunother Cancer*, 9(1). doi: 10.1136/jitc-2020-001136

28. Ding, Q., Dong, S., Wang, R. *et al.*, 2020, A nine-gene signature related to tumor microenvironment predicts overall survival with ovarian cancer. *Aging (Albany NY)*, 12(6):4879-4895. doi: 10.18632/aging.102914

29. Di Modugno, F., Colosi, C., Trono, P. *et al.*, 2019, 3D models in the new era of immune oncology: focus on T cells, CAF and ECM. *J Exp Clin Cancer Res*, 38(1):117. doi: 10.1186/s13046-019-1086-2

30. Hinshaw, D. C. & Shevde, L. A., 2019, The Tumor Microenvironment Innately Modulates Cancer Progression. *Cancer Res*, 79(18):4557-4566. doi: 10.1158/0008-5472.CAN-18-3962

31. Elhanani, O., Ben-Uri, R. & Keren, L., 2023, Spatial profiling technologies illuminate the tumor microenvironment. *CANCER CELL*, 41(3):404-420. doi: 10.1016/j.ccell.2023.01.010

32. Wei, X., Lou, H., Zhou, D. *et al.*, 2021, TAGLN mediated stiffness-regulated ovarian cancer progression via RhoA/ROCK pathway. *J Exp Clin Cancer Res*, 40(1):292. doi: 10.1186/s13046-021-02091-6

33. Kim, J., Jang, J. & Cho, D. W., 2021, Controlling Cancer Cell Behavior by Improving the Stiffness of Gastric Tissue-Decellularized ECM Bioink With Cellulose Nanoparticles. *Front Bioeng Biotechnol*, 9:605819. doi: 10.3389/fbioe.2021.605819

34. Tang, M., Tiwari, S. K., Agrawal, K. *et al.*, 2021, Rapid 3D Bioprinting of Glioblastoma Model Mimicking Native Biophysical Heterogeneity. *Small*, 17(15):e2006050. doi: 10.1002/smll.202006050

35. Yang, X., Wang, G., Huang, X. *et al.*, 2020, RNA-seq reveals the diverse effects of substrate stiffness on epidermal ovarian cancer cells. *Aging (Albany NY)*, 12(20):20493-20511. doi: 10.18632/aging.103906

36. Pietilä, E. A., Gonzalez-Molina, J., Moyano-Galceran, L. *et al.*, 2021, Co-evolution of matrisome and adaptive adhesion dynamics drives ovarian cancer chemoresistance. *Nat Commun*, 12(1):3904. doi: 10.1038/s41467-021-24009-8

37. Ouyang, L., Yao, R., Zhao, Y. *et al.*, 2016, Effect of bioink properties on printability and cell viability for 3D bioplotting of embryonic stem cells. *Biofabrication*, 8(3):035020. doi: 10.1088/1758-5090/8/3/035020

38. Li, C., Jin, B., Sun, H. *et al.*, 2022, Exploring the function of stromal cells in cholangiocarcinoma by three-dimensional bioprinting immune microenvironment model. *Front Immunol*, 13:941289. doi: 10.3389/fimmu.2022.941289

39. Singha, B., Gatla, H. R., Manna, S. *et al.*, 2014, Proteasome inhibition increases recruitment of IκB kinase β (IKKβ), S536P-p65, and transcription factor EGR1 to interleukin-8 (IL-8) promoter, resulting in increased IL-8 production in ovarian cancer cells. *J Biol Chem*, 289(5):2687-2700. doi: 10.1074/jbc.M113.502641

40. Javellana, M., Eckert, M. A., Heide, J. *et al.*, 2022, Neoadjuvant Chemotherapy Induces Genomic and Transcriptomic Changes in Ovarian Cancer. *Cancer Res*, 82(1):169-176. doi: 10.1158/0008-5472.CAN-21-1467

41. du Manoir, S., Delpech, H., Orsetti, B. *et al.*, 2022, In high-grade ovarian carcinoma, platinum-sensitive tumor recurrence and acquired-resistance derive from quiescent residual cancer cells that overexpress CRYAB, CEACAM6, and SOX2. *J Pathol*, 257(3):367-378. doi: 10.1002/path.5896

42. Yamawaki, K., Mori, Y., Sakai, H. *et al.*, 2021, Integrative analyses of gene expression and chemosensitivity of patient-derived ovarian cancer spheroids link G6PD-driven redox metabolism to cisplatin chemoresistance. *Cancer Lett*, 521:29-38. doi: 10.1016/j.canlet.2021.08.018

43. Kang, Y., Nagaraja, A. S., Armaiz-Pena, G. N. *et al.*, 2016, Adrenergic Stimulation of DUSP1 Impairs Chemotherapy Response in Ovarian Cancer. *Clin Cancer Res*, 22(7):1713-1724. doi: 10.1158/1078-0432.Ccr-15-1275

44. Andreoli, M., Persico, M., Kumar, A. *et al.*, 2014, Identification of the first inhibitor of the GBP1:PIM1 interaction. Implications for the development of a new class of anticancer agents against paclitaxel resistant cancer cells. *J Med Chem*, 57(19):7916-7932. doi: 10.1021/jm5009902

45. Xiao, Y., Lai, Y., Yu, Y. *et al.*, 2021, The Exocrine Differentiation and Proliferation Factor (EXDPF) Gene Promotes Ovarian Cancer Tumorigenesis by Up-Regulating DNA Replication Pathway. *Front Oncol*, 11:669603. doi: 10.3389/fonc.2021.669603

46. Zhang, Y., Qiu, J. G., Jia, X. Y. *et al.*, 2023, METTL3-mediated N6-methyladenosine modification and HDAC5/YY1 promote IFFO1 downregulation in tumor development and chemo-resistance. *Cancer Lett*, 553:215971. doi: 10.1016/j.canlet.2022.215971

47. Zaid, T. M., Yeung, T. L., Thompson, M. S. *et al.*, 2013, Identification of FGFR4 as a potential therapeutic target for advanced-stage, high-grade serous ovarian cancer. *Clin Cancer Res*, 19(4):809-820. doi: 10.1158/1078-0432.Ccr-12-2736

48. Brancato, V., Oliveira, J. M., Correlo, V. M. *et al.*, 2020, Could 3D models of cancer enhance drug screening? *BIOMATERIALS*, 232:119744. doi: 10.1016/j.biomaterials.2019.119744

49. Zanoni, M., Cortesi, M., Zamagni, A. *et al.*, 2020, Modeling neoplastic disease with spheroids and organoids. *J Hematol Oncol*, 13(1): 97. doi: 10.1186/s13045-020-00931-0

50. Fan, Y., Sun, Q., Li, X. *et al.*, 2021, Substrate Stiffness Modulates the Growth, Phenotype, and Chemoresistance of Ovarian Cancer Cells. *Front Cell Dev Biol*, 9:718834. doi: 10.3389/fcell.2021.718834

51. Paradiso, F., Lenna, S., Gazze, S. A. *et al.*, 2022, Mechanomimetic 3D Scaffolds as a Humanized In Vitro Model for Ovarian Cancer. *Cells*, 11(5). doi: 10.3390/cells11050824

52. Barroso, M., Chheda, M. G., Clevers, H. *et al.*, 2022, A path to translation: How 3D patient tumor avatars enable next generation precision oncology. *CANCER CELL*, 40(12):1448-1453. doi: 10.1016/j.ccell.2022.09.017

53. Kim, J., Koo, B. K. & Knoblich, J. A., 2020, Human organoids: model systems for human biology and medicine. *Nat Rev Mol Cell Biol*, 21(10):571-584. doi: 10.1038/s41580-020-0259-3

54. Zanella, E. R., Grassi, E. & Trusolino, L., 2022, Towards precision oncology with patient-derived xenografts. *Nat Rev Clin Oncol*, 19(11):719-732.
doi: 10.1038/s41571-022-00682-6

55. Zhuo, J., Su, R., Tan, W. *et al.*, 2020, The ongoing trends of patient-derived xenograft models in oncology. *Cancer Commun (Lond)*, 40(11):559-563.
doi: 10.1002/cac2.12096

56. Zong, X., Wang, W., Ozes, A. *et al.*, 2020, EZH2-Mediated Downregulation of the Tumor Suppressor DAB2IP Maintains Ovarian Cancer Stem Cells. *Cancer Res*, 80(20):4371-4385.
doi: 10.1158/0008-5472.Can-20-0458

57. Sacks Suarez, J., Gurler Main, H., Muralidhar, G. G. *et al.*, 2019, CD44 Regulates Formation of Spheroids and Controls Organ-Specific Metastatic Colonization in Epithelial Ovarian Carcinoma. *Mol Cancer Res*, 17(9):1801-1814.
doi: 10.1158/1541-7786.Mcr-18-1205

58. Zhao, Y., He, M., Cui, L. *et al.*, 2020, Chemotherapy exacerbates ovarian cancer cell migration and cancer stem cell-like characteristics through GLI1. *Br J Cancer*, 122(11):1638-1648.
doi: 10.1038/s41416-020-0825-7

59. Wang, Y., Niu, X. L., Qu, Y. *et al.*, 2010, Autocrine production of interleukin-6 confers cisplatin and paclitaxel resistance in ovarian cancer cells. *Cancer Lett*, 295(1):110-123.
doi: 10.1016/j.canlet.2010.02.019

60. Klinghammer, K., Walther, W. & Hoffmann, J., 2017, Choosing wisely - Preclinical test models in the era of precision medicine. *Cancer Treat Rev*, 55:36-45.
doi: 10.1016/j.ctrv.2017.02.009